Structures 3 (2015) 250–260

Contents lists available at ScienceDirect

Structures

journal homepage: http://www.elsevier.com/locate/structures

Improved Formulation of Travelling Fires and Application to Concrete and Steel Structures

Egle Rackauskaite [a], Catherine Hamel [a,b], Angus Law [c], Guillermo Rein [a,*]

[a] Department of Mechanical Engineering, Imperial College London, UK
[b] Department of Fire Protection Engineering, University of Maryland, College Park, USA
[c] Arup, UK

ARTICLE INFO

Article history:
Received 19 March 2015
Received in revised form 2 June 2015
Accepted 3 June 2015
Available online 11 June 2015

Keywords:
Fire resistance
Travelling fires
Steel
Concrete
Structures in fire

ABSTRACT

Current design codes and consequently most of the understanding of behaviour of structures in fire are based on the often unrealistic assumption of uniform fire within the enclosure. This assumption is especially wrong in the case of large open-plan compartments, where non-uniform travelling fires have been observed instead. An innovative concept called the Travelling Fires Methodology (TFM) has been developed to take into account this non-uniform fire behaviour. In this study, TFM has been improved to account for better fire dynamics. Equations are introduced to reduce the range of possible fire sizes taking into account fire spread rates from real fires. The analytical equations used to represent the far-field temperatures are presented in continuous form. The concept of flame flapping is introduced to account for variation of temperatures in the near-field region due to natural fire oscillations. These updated near-field temperatures cover a range of temperatures between 800 and 1200 °C, depending on fire size and compartment characteristics. These incorporated changes are based on a fire model which can be used flexibly and adjusted to fit experimental data when it becomes available in the near future. Improved TFM (iTFM) is applied to generic concrete and steel compartments to study the effect of non-uniform heating associated with the travelling fires by investigating the location of the peak temperature along the fire path. It is found to be mainly dependent on the fire spread rate and the heat release rate. Location of the peak temperature in the compartment mostly occurs towards the end of the fire path.

1. Introduction

Accidental fire can be disastrous, especially in buildings. Most fire deaths occur due to the toxic effects of smoke before any structural collapse [1]. However, the effect of fire on structural stability is critical in regard to safe evacuation and safe access for fire fighters, financial losses, and lost business. This is particularly the case in tall buildings where extended evacuation times are required due to phased evacuation practices [2].

Innovative architectural designs of modern buildings already provide a challenge to structural engineers. This is above all the case in structural fire engineering [3,4]. Understanding of fundamental mechanisms of whole building behaviour in fire has significantly increased in the last decades, especially after full-scale tests of various multi-storey buildings were carried out in Cardington between 1994 and 1999 [5,6]. However, most of this understanding and current design codes are based on the assumption of uniform fires in a compartment. An extensive recent work [7,8] has shown that while the uniform fire assumption may be suitable for small enclosures, fires in large, open-plan compartments, typical of modern architecture, do not cover the full area of compartment but rather travel from one part of it to another with non-uniform temperature distribution. These fires are referred to as *travelling fires*.

Current design standards (e.g. Eurocodes) do not account for such fires. The standard fire and parametric time–temperature curves are based on small scale tests (<100 m^2 [9]), and assume uniform burning of fire and homogeneous temperature distributions in the compartment. In large accidental events, fires have been observed to travel across floor plates and between storeys. Accidental events where fires were observed to travel include World Trade Centre Towers 1, 2 & 7 (2001); Windsor Tower fire in Madrid (2006); Faculty of Architecture building fire at TU Delft (2008); Interstate Bank fire in Los Angeles (1988); and One Meridian Plaza fire in Philadelphia (1991). In all of these accidents, the fires lasted for up to 7 or even 20 hours (i.e. Windsor Tower and Meridian Plaza fires). Such long fire durations are not considered nor can be understood by current design codes. It has been shown in the WTC Towers study by NIST [10,11] that such prolonged periods of heating may result in even protected structural elements reaching temperatures in excess of 600 °C. They also concluded that using average uniform gas temperatures rather than travelling fires would have led

* Corresponding author.
E-mail address: g.rein@imperial.ac.uk (G. Rein).

http://dx.doi.org/10.1016/j.istruc.2015.06.001

Nomenclature

A_f	surface area of burning fuel [m^2]
H	height of the compartment [m]
L	length of the compartment [m]
L_f	length of the design area involved in fire [m]
$L_{f,max}$	maximum possible fire size in terms of length along the fire path [m]
$L_{f,min}$	minimum fire size in terms of length along the fire path [m]
L^*	dimensionless design fire size
L_t^*	varying dimensionless fire size which depends on the location of the leading edge
$Q^{\bullet}$	total heat release rate [kW]
$Q^{\bullet''}$	heat release rate per unit area [kW/m^2]
T_f	reduced near-field temperature due to flapping [°C]
T_{ff}	far-field temperature [°C]
T_{max}	gas temperature [°C]
T_{nf}	near-field temperature [°C]
T_∞	room temperature [°C]
W	width of the compartment [m]
θ	flapping angle [°]
f	flapping length [m]
q_f	fuel load density [kJ/m^2]
r	radial distance away from the fire [m]
s	fire spread rate [m/s]
s_{max}	maximum realistic fire spread rates in building fires [m/s]
s_{min}	minimum realistic fire spread rates in building fires [m/s]
t	time [s]
t_b	local burning time [s]
t_{total}	total fire duration [s]
x	location of interest in the compartment [m]
$x^{\bullet}$	location of the leading edge of the fire relative to the end of compartment where fire started [m]
x^*	dimensionless location in the compartment along the fire path

to significant errors in subsequent thermal and structural analysis of collapse of WTC Towers.

The need and urge of new design methods to incorporate realistic behaviour of fires in large open-plan offices have been highlighted recently [12]. Clifton [13] was the first person to introduce the approach for the development of temperature–time relationships which would consider travelling fires. It was published as a part of HERA programme reports in New Zealand. Clifton's approach splits the compartment (firecell) into four distinct regions at any one time: preheat, fire, burned out and smoke logged. However, the model has not been developed or used further.

Recently, an extensive work has been done by Stern-Gottfried, Law and Rein [7,8,14,15] who have developed a new design concept of Travelling Fires Methodology (TFM). It considers non-uniform temperature distributions along the compartment and a wide range of fire sizes (burning floor area). The concept has already been applied by Engineering Consultant, Arup. In the published work [16,17] on Arup's approach, the limitations of only using prescriptive codes for the design have been identified. Travelling fires were accounted in probabilistic analysis to identify the most severe fire scenario in regard to fire resistance periods. New Ludgate, a 10 storey office development in the City of London, was described as a case study in [16]. In order to determine the optimum structural fire protection specification in accordance with Part B of the UK Building Regulations, the structural fire performance was expressed in terms of reliability according to Kirby et al. [18]. Thus, a probabilistic Monte Carlo analysis was carried out by varying the types of fires that are likely to occur (i.e. uniform and travelling fires) and the corresponding key parameters. These parameters include fuel load, heat release rate and fire size. The resultant structural reliability was combined with sprinkler reliability to find the corresponding required fire resistance period based on steel temperature. The use of travelling fires in addition to uniform fires in a building design as in the above approach allows a better understanding of the overall building performance subject to a range of conditions.

The focus of this paper is the improvement of the TFM to account for better fire dynamics, smaller range of fire sizes and the analysis of the effect of non-uniform heating associated with travelling fires on the temperatures of structural members. The proposed changes represent a simple yet powerful fire model which can be used flexibly and adjusted to fit experimental data when it becomes available in the near future.

2. Travelling Fires Methodology

The Travelling Fires Methodology (TFM) was developed by Stern-Gottfried, Law and Rein [7,8,14]. This framework incorporates the effect of non-uniform fires in large open-plan spaces. It does not supersede traditional design methods, but can be used in addition to them, and investigates a range of possible fire dynamics instead of just one or two design fires.

TFM provides an approach for generation of gas temperature–time curves at the ceiling of a medium height compartment at any location in the compartment. The ceiling is the target because this is where maximum temperatures are expected. TFM considers design fires to be composed of two moving regions: the near-field (flames) and the far-field (smoke). An illustration of the two fields is shown in Fig. 1. The near-field represents the flames directly impinging on the ceiling and assumes the peak flame temperatures. The far-field model represents smoke temperatures which decrease with distance away from the fire due to mixing with air. Any structural element will experience cooler far-field temperatures which correspond to pre-heating and/or cooling for much longer duration than the short hotter near-field. Test data from the St. Lawrence Burns large compartment tests conducted in 1958 support travelling fire behaviour as in TFM framework [19,20].

Early work by Rein et al. [15] employed computational fluid dynamics to generate temperature fields. Later it was simplified for a single floor in order to pass less information to consequent structural analysis but still provide realistic results. It used a ceiling jet correlation to describe the temperature field. The methodology was then extended and various parameter sensitivity analyses were carried out by investigating the structural behaviour of a general concrete frame [8]. In the present study the thermal descriptions of near-field and far-field temperatures used in TFM and the possible range of valid fire sizes are reduced. Also, the thermal response to travelling fires of two structurally equivalent steel and concrete beams is studied. For clarity, the previous version [8] of Travelling Fires Methodology is referred to as TFM and the Travelling Fires Methodology with improved formulations presented in this paper is referred to as iTFM.

3. Improved Travelling Fires Methodology — iTFM

3.1. Valid range of fire sizes

TFM is flexible in a way that it is not limited to one fire type. It covers a wide range of fire sizes — a family of possible fires depending on the fire coverage of the total floor area from 1% to 100%. The latter represents the whole compartment under uniform fire. In Eurocode 1 Part 1-2 consideration is given to only two different fire sizes: a whole compartment fire (100%), and a static localised fire up to 10 m in diameter. TFM assumes uniform fuel load distribution along the fire path and constant fire spread rate. Therefore, the total fire duration depends on the fire size. For example, for a floor area of 960 m^2, the fire size can range from 38 min for 100% fire size, to 1919 min for 1% (or even longer depending on compartment and fuel load characteristics). Thus, unlike

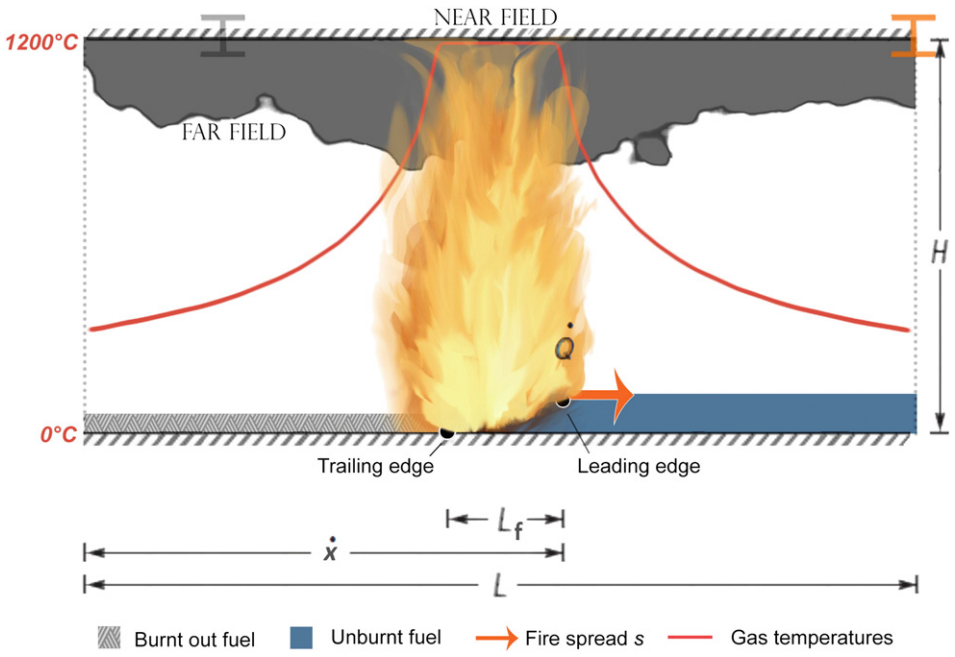

Fig. 1. Illustration of a travelling fire and distribution of gas temperatures.

traditional design methods, TFM can explain and takes into account the long fire durations observed in accidental fires.

However, it is unlikely that a very thin line fire (e.g. 1%) across the whole width of the compartment would spread, or that a whole floor (e.g. 2500 m^2) would be involved at once in fire in large compartments. This is due to limitations such as available fuel load, fire spread rate and burning rate. The aim in the present study is to provide a better representation of physically possible fire sizes which were not limited in the previous versions of TFM.

In TFM a fire is assumed to be fuel controlled. It was identified in the previous work [5–6] that ventilation controlled fires are unlikely in large enclosures. Therefore, fuel load density, q_f, and heat release rate per unit area, $Q^{\bullet''}$, are used as main design variables. A range of possible values for these parameters for different building occupancies can be found in the Eurocode [21]. Based on these values a local burning time, t_b, is calculated (e.g. 19 min) using Eq. (1). This variable quantifies the time needed for an area involved in fire to burn out completely.

$$t_b = q_f / Q^{\bullet''} \tag{1}$$

The front of a travelling fire is referred to as the leading edge (see Fig. 1). The leading edge location is determined using the fire spread rate. If the range of the realistic fire spread rates is known it can be used to compute the limiting sizes of possible fires. This can be done by finding the distance that the leading edge of the fire would travel before burning out at the ignition point as in Eq. (2):

$$L_{f,min/max} = s_{min/max} \cdot t_b \tag{2}$$

where $L_{f,min/max}$ is the minimum or maximum possible fire size in terms of length along the fire path (m); and $s_{min/max}$ is the minimum or maximum realistic fire spread rate in building fires (m/s). Available data on typical compartment fire spread rates is very limited. Thus, estimates were made based on the details provided in a number of fire tests and real building fire investigation reports where the fires have been observed to travel [11,19,20,22–26]. A summary of the reported fire spread rates and estimated values is shown in Table 1.

From the limited data it can be seen that fire spread rates in the open for wood cribs (a typical fuel source used for fire tests) and in compartments typically vary between 0.1 and 19.3 mm/s. These values are suggested as minimum and maximum fire spread rates for the determination of a valid range of fire sizes. Clifton [13] assumed the values of 8.3 and 16.6 mm/s for slow and fast fire spread respectively based on the results from the tests on natural fires in large scale compartments [25] and a rate of fire spread between different workstations of 200 s given by [27]. These values agree well with the suggested range for the iTFM. Based on the limitations from realistic fire spread rates, valid range of fire sizes can be described as below:

$$\text{from } \frac{L_{f,min}}{L} \text{ to } \frac{L_{f,max}}{L}.$$

As experimental evidence becomes available (presently not available), the range of possible fire spread rates in compartments can be updated as appropriate. The valid range of fire sizes is necessary to reduce the family of fires passed to structural analysis, reduce computational time and neglect unrealistic results.

3.2. Far-field — the analytical solution

In TFM the far-field model represents cooler smoke temperatures which decrease with distance away from the fire. TFM is flexible in stating that any available temperature–distance correlation could be used to describe the far-field temperature depending on the accuracy required. Alpert's ceiling jet correlation [28], which is based on a set of

Table 1
Realistic fire spread rates, s, based on data from experiments and real fires.

Reference	Details	Spread rates (mm/s)
[23]	Wood cribs in the open	0.1–2
[24]	Lateral or downward spread on thick solids	1
[25]	Tests on natural fires in large scale compartments	1.5–19.3
[11]	Reconstruction of WTC fires (2001)	2.5–16.7
[19,20]	St. Lawrence Burns tests (1958)	7.5–13
[22,26]	First Interstate Bank fire (1988)	14.5

experiments created for sprinkler design, is used in TFM to represent the far-field temperatures. It is shown in Eq. (3).

$$T_{max} - T_{\infty} = 5.38\left(\frac{Q^{\bullet}/r)^{2/3}}{H}\right. \tag{3}$$

The first version of TFM used a single far-field temperature [15] and then to incorporate radiative heat transfer the 4th power average was used [14]. In the last version [8], TFM assumes the compartment to be divided into discrete nodes and uses gas temperatures that vary with distance from fire. The use of compartment floor discretization adds unnecessary complexity to the problem. Moreover, in a parameter sensitivity study [8], errors of up to 12.7% and 20% were found for peak rebar bay temperatures and total burning durations respectively, depending on the grid size chosen.

Recently, a few new methods for the calculation of ceiling-jet temperatures have been proposed based on computational simulations [29,30]. Suzuki [29] created a new model by expanding Alpert's theory [31] to include terms that account for time considerations and the heat transfer to the ceiling. The resultant temperatures showed no significant differences from Alpert's correlation [28] and were slightly lower than the values predicted by Heskestad [32]. In [29] comparisons were also made to a full-scale experiment in an office building and calculated values were found to be lower by 10–25% in some cases. Suzuki [29] concluded that this may be due to the presence of a side wall which was not included in the model. In the recent work by Johansson et al. [30], 90 computational simulations were performed to study ceiling-jet temperatures. The resultant average ceiling jet temperatures compared well with Alpert's ceiling jet correlation [28]. However, this was not the case for recorded maximum temperatures and a new correlation was developed.

Both of the models identified previously require additional variables in comparison to the simpler Alpert's correlation for the calculation of ceiling jet temperatures. However, taking into account the additional complexity, computational time required and uncertainty in the parameters associated with these two methods, the differences in resultant temperatures are negligible. Thus, for reasons of simplicity, the far-field model in iTFM continues to be based on Alpert's correlation [28]. iTFM has been improved by developing the analytical expression for the far-field temperatures, thus removing the errors that were imposed using the discrete method. The proposed equations can be used to rapidly calculate temperature variations at any time and location along the structural member in the compartment.

TFM assumes a uniform fuel load across the fire path (q_f) and constant heat release rate ($Q^{\bullet''}$). Also, the fire is defined by a specified surface area of burning fuel, A_f, at any fixed time. Considering this, the total heat release rate can be calculated by the following equation:

$$Q^{\bullet} = A_f \cdot Q^{\bullet''}. \tag{4}$$

To consider fire growth and decay and to represent varying fire size at the beginning and end of the fire, respectively, the following equation can be used:

$$A_f = L \cdot L_t^{*} \cdot W \cdot Q^{\bullet''}. \tag{5}$$

where L_t^{*} is the varying dimensionless fire size which depends on the location of the leading edge of the fire $x^{\bullet}$; L (m) is the length of the compartment; and W (m) is the width of the compartment. Dimensionless design fire size L^{*}, fire spread rate s (m/s), total fire duration t_{total} (s), and location of the leading edge of the fire relative to the end of the compartment where the fire started $x^{\bullet}$ (m) can be calculated as follows:

$$L^{*} = L_f/L \tag{6}$$

$$s = L_f/t_b \tag{7}$$

$$t_{total} = t_b(1/L^{*} + 1) \tag{8}$$

$$x^{\bullet} = s \cdot t \tag{9}$$

where L_f (m) is the design length of the area involved in fire and t (s) is time.

Combining Eqs. (3)–(9) results in a correlation for gas temperatures T_{max} at a location x and time t of interest:

$$T_{max}(x,t) = T_{\infty} + \frac{5.38}{H}\left(\frac{L\,L_t^{*}\,W\,Q^{\bullet''}}{x + 0.5\,L\,L_t^{*} - x^{\bullet}{}_t)}\right.^{2/3} \tag{10}$$

$$T_{max}(x,t) = T_{nf}, \text{ if } \begin{cases} T_{ff} > T_{nf}; \\ x + 0.5\,L\,L_t^{*} - x^{\bullet}{}_t \le 0.5 L_f \end{cases} \tag{11}$$

$$\text{for } x^{\bullet} \le L \rightarrow x^{\bullet}{}_t = s \cdot t;\ L_t^{*} = \min[L^{*}, (s \cdot t)/L] \tag{12}$$

$$x^{\bullet} > L \rightarrow x^{\bullet}{}_t = \mathrm{L}; \qquad L_t^{*} = 1 + (L_f - s \cdot t)/L. \tag{13}$$

Conditions described by Eq. (11) represent the near-field temperature. It implies that far-field temperatures cannot exceed the near-field flame temperature. It also sets the near-field temperature value for the whole length of the area involved in fire (L_f). Eqs. (12) and (13) are used to define varying fire size and location of the leading edge based on whether fire is still increasing in size or is at its maximum size (Eq. (12)) or has reached the far end of the compartment and is decaying (Eq. (13)). Illustrative examples of resulting gas temperature surroundings experienced by structural members at two different locations within a typical compartment are shown in Fig. 2.

3.3. Near-field — flame flapping

In TFM the near-field represents the flames directly impinging on the ceiling and assumes the peak flame temperatures. Such temperatures in various building fires and experiments have been measured in the range of 800–1200 °C [33–36]. To stay on the conservative side TFM described in [8,14,15] assumed the near-field temperature to be 1200 °C.

In reality, due to natural lateral fluctuations of the flames on the ceiling, gas temperatures are typically continuously varying between the observed temperatures of 800 and 1200 °C [24,37,38]. In iTFM this is included and referred to as *flame flapping*. For this reason, structural members will actually experience lower average gas temperatures rather than the peak flame temperatures observed in fires. There is no experimental evidence from large compartment fires or correlations based on which this reduced near-field temperature could be related to either fire size or oscillations. In previous work of TFM [8,14] this was indirectly

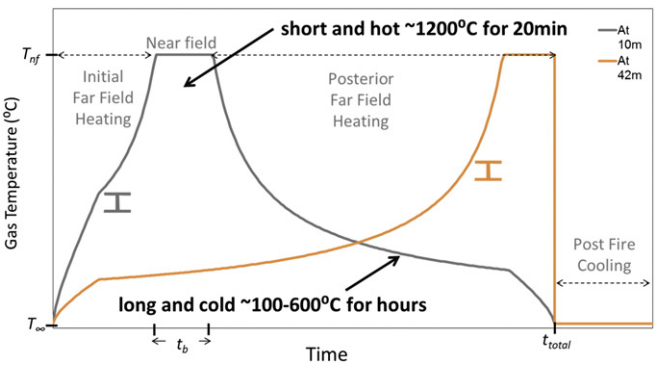

Fig. 2. Near-field and far-field exposure duration at an arbitrary location [8] and at the far end of the compartment.

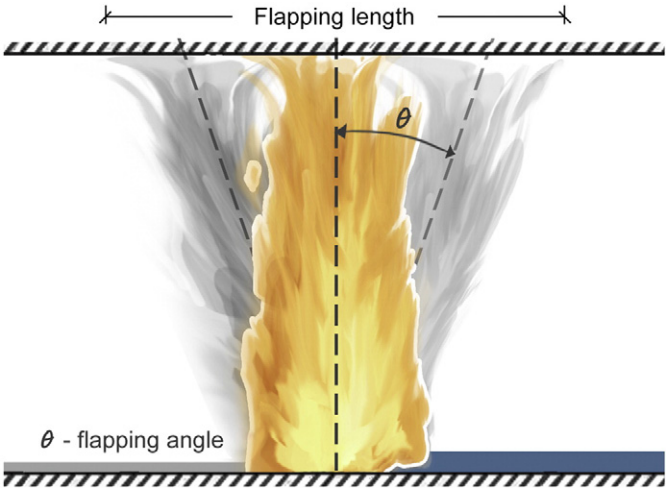

Fig. 3. Representation of the flapping length (f) on the ceiling and angle (θ).

taken into account by calculating the average bay temperatures for structural members. However, this assumption and its implications were not studied. In order to apply reduced near-field temperatures due to flapping for iTFM, the concept of the flapping angle is introduced. The angle from the main axis of the flame (θ), as shown in Fig. 3, is chosen to represent the length on the ceiling over which fluctuations of the impinging flame occur.

The review of available data on flapping angles is discussed in Appendix A. For iTFM the flapping angle of $\pm 6.5°$ was chosen based on results from Quintiere et al. [39] experiments (see Appendix A). The flapping angle is used to calculate the ceiling length over which the impinging fire fluctuations occur. The average temperature over this length (f) is calculated accounting for both far-field and peak near-field temperatures (set at 1200 °C). This represents the mixing of cooler smoke with the fluctuating flame, resulting in a lower near-field temperature. This reduced near-field temperature is used to generate travelling fire time–temperature curves instead of a fixed peak value of 1200 °C. The equation used to calculate the reduced near-field temperature due to flapping is

Table 2
Details of the steel and concrete sections used for the case study.

Fire resistance	457 × 191 UB133 Steel protection thickness (m)	500 × 300 Rebar cover (m)
60 min	0.007	0.038
120 min	0.018	0.042

shown below and is derived from Alpert's ceiling jet correlation. For derivation see Appendix B.

$$T_f = T_\infty + \frac{T_{nf}(2r_{x1} + L_f) - 2T_\infty \cdot r_{x2}}{f} + \frac{32.28Q^{*2/3}}{H \cdot f}\left(r_2{}^{1/3} - r_{x2}{}^{1/3}\right) \quad (14)$$

where

$$r_2 = f/2 \quad (15)$$

$$r_{x1} = \max[0, r_0 - L_f/2] \quad (16)$$

$$r_{x2} = \max[L_f/2, r_0] \quad (17)$$

$$T_{nf} = 1200°\mathrm{C} \quad (18)$$

$$r_0 = \left(\frac{5.38}{H(T_{nf} - T_\infty)}\right)^{3/2}. \quad (19)$$

Variation of reduced near-field temperatures with flapping angle for different fire sizes is shown in Fig. 4. It can be seen that with increasing flapping angle the resulting temperature for each fire size decreases. This could be expected as a larger flapping length incorporates a greater amount of smoke in comparison to direct flame impingement. Thus, due to the mixing of these two fields, the resulting gas temperatures are lower. Fig. 4 also shows that the effect of flapping angle is only important for smaller fire sizes (<12%) as these are more susceptible to the flapping disturbances. Also, flapping leads to reduced near-field temperatures in the range of 800–1200 °C, in agreement with observed temperatures in real fires. All of this considered, this is still a crude approximation and more research on peak flame temperatures in relation to fire size in large enclosures is necessary.

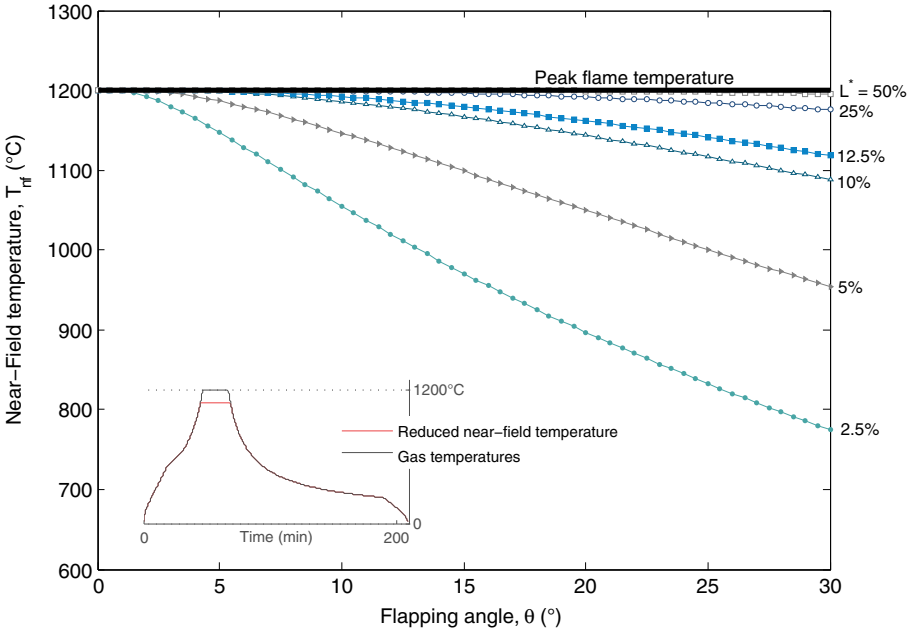

Fig. 4. Variation of reduced near-field temperature with flapping angle and fire size.

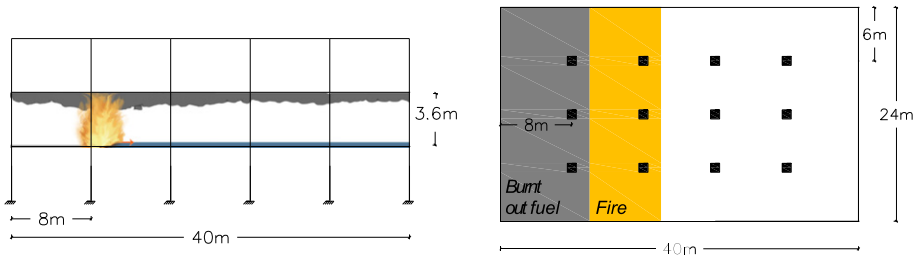

Fig. 5. Elevation and floor plan building use for the case study.

4. Case study

To investigate the impact of iTFM on resulting temperatures within structural members, it was applied to the steel and concrete frames. A given floor was assumed to be 24 m wide, 40 m long and 3.6 m high as for a typical office building. It was divided into 5 spans along the compartment length, each 8 m long. Simply supported steel and concrete beams were designed in accordance with Eurocode 3 [40] and Eurocode 2 [41], respectively, for the same factored uniformly distributed load of 56.4 kN/m. Thus, the two sections can be considered as structurally equivalent. Each of the sections was also designed for 60 min and 120 min fire resistance (typical resistance requirements for office buildings). Steel insulation properties were taken as for high density perlite (thermal conductivity k_i = 0.12 W/m K, density ρ_i = 550 kg/m^3 and specific heat c_i = 1200 J/kg K) [3]. The details of the designed sections are shown in Table 2 and Fig. 5.

Heat release rate per unit area and fuel load density were assumed to be 500 kW/m^2 and 570 MJ/m^2 respectively [8]. A base case flapping angle of 6.5° was chosen. Time–temperature gas curves obtained from iTFM were used as an input for a heat transfer analysis to heated beams. All heat transfer calculations were carried out as in [8]. Lumped mass heat transfer method [3] was used to calculate resulting steel beam temperatures. The convective heat transfer coefficient, density of steel and radiative emissivity were assumed to be 35 W/m^2 K, 7850 kg/m^3 and 0.7, respectively [3,8,21]. In-depth concrete temperatures were calculated using explicit one-dimensional finite difference model for heat conduction. Radiation and convection were taken into account for the boundary conditions. The density of concrete of 2300 kg/m^3, the specific heat of concrete of 1000 J/kg K, convective heat transfer coefficient for the exposed surface of 35 W/m^2 K, convective heat transfer coefficient for the backside surface of 4 W/m K, thermal conductivity of concrete of 1.3 W/m K and a radiative emissivity of 0.7 were assumed [3,8,21]. Steel has a much higher thermal conductivity coefficient than concrete. Thus, steel rebar was assumed to have the same temperature as adjacent concrete. Time steps used for heat transfer calculations satisfying the stability criteria were 10 s [3,8] and 1.9 s [8,42] for steel and concrete respectively. An in-depth concrete grid size of 0.002 m, which meets stability criteria [8,42], was chosen.

4.1. Valid range of fire sizes

As identified in Section 3.1 limiting fire sizes for the case study have been calculated based on the fire spread rates. The resultant values are shown in Table 3.

Valid fire sizes are in the range between 0.3% and 55%. This leads to the elimination of half of the fire sizes range used in previous TFM, thus reducing required analysis times. This also indicates, as mentioned previously, that very small fire sizes (i.e. thin fires) and well-ventilated fires covering a whole floor area are unlikely to occur in large compartments unless a lower heat release rate is assumed. From Fig. 6, it can be clearly seen that lower heat release rates result in larger fire sizes as a result of longer local burning durations. Minimum fire sizes are unrealistically low and almost constant for all fuel load densities as it is based on very small spread rates from wood crib fires. This also indicates that much research on flame spread rates is still needed in order to gain a better understanding of fire dynamics and optimise fire curves for structural design further.

Table 3
Valid range of fire sizes for the case study.

Limitation	Minimum fire length $L_{f,min}$ (m)	Maximum fire length $L_{f,max}$ (m)
Spread rates (0.1–19.3 mm/s)	0.11 (0.3%)	22.00 (55%)

4.2. Flapping angle

In previous TFM studies [8,14] it was identified that the fire sizes between 5 and 20% result in highest peak member temperatures. The influence of the varying flapping angles defined in Section 3.3 on the peak steel and concrete temperatures with increasing fire size can be seen in Fig. 7. Clearly, the highest peak temperatures at the smallest fire sizes dissipate with increasing flapping angle (i.e. decreasing near-field temperature). It indicates that the effect of fire spread rate is less dominant at lower near-field temperatures due to a smaller heat flux. Also, flapping influence diminishes with fire sizes larger than 20%, 25% and 30% for 120 min protected steel beam, 60 min protected steel beam, and concrete and unprotected steel beams respectively. The thermal protection of structural members results in the delayed heating. Thus, the thicker the protection, the narrower the range of fire sizes which result in highest peak member temperatures.

Due to lower thermal conductivity, the resultant peak temperatures in concrete rebar are approximately 600 °C lower than in unprotected steel beam. In this case concrete rebar peak temperatures are between the limits of peak temperatures in 60 min protected and 120 min protected steel beam. For the same reason the thickness of concrete cover has little influence. For 60 min and 120 min fire protection the

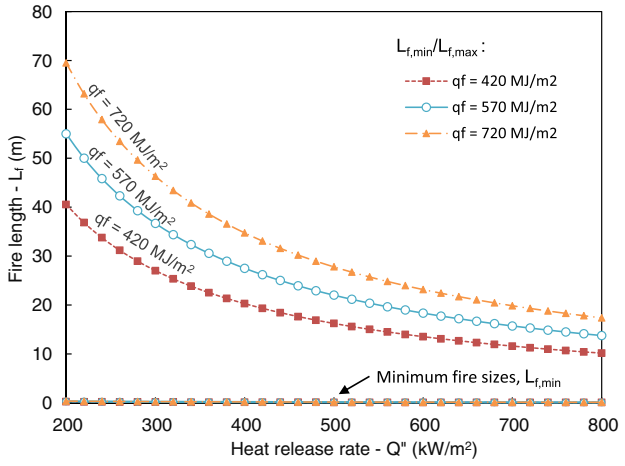

Fig. 6. Valid range of fire sizes for varying heat release rates and fuel load densities.

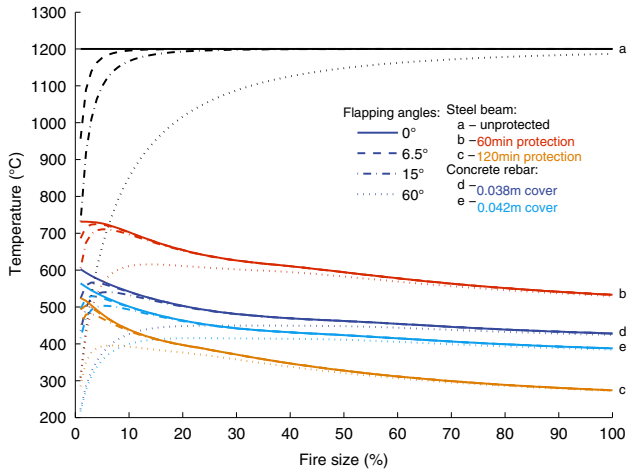

Fig. 7. Influence of flapping angle on variation of peak steel and concrete temperatures with fire size.

difference in concrete rebar temperatures is approximately 40 °C while for steel beams it is up to 250 °C. On the other hand, variations in flapping angle have a similar influence on both steel and concrete temperatures, which can cause variations up to 200 °C. However, structural analysis has to be carried out in order to make a valid comparison of steel and concrete beam structural resistance in fire.

4.3. Location of peak temperature in the compartment

Overall structure performance in a real fire depends on a number of factors. They include temperature rise, loading, restraint, composite action effects and continuity within the structure [43]. In this study the location of the peak temperature in the compartment as a result of iTFM is studied. This is to give an insight of how non-uniform heating associated with a spreading fire would affect the resultant structural member temperatures. The general conclusions drawn herein may be important for the identification of critical structural members within the structure.

Location of the peak temperature within steel beam in the compartment was investigated by varying various iTFM parameters. They include the length of the compartment L, thickness of fire protection, heat release rate per unit area $Q^{\bullet''}$, fuel load density q_f, and flapping angle θ. Variation of peak temperatures along the fire path in the compartment is shown in Fig. 8. These temperatures represent the highest temperatures reached in different locations during the fire. They do not represent temperature distribution occurring at the same time during the fire in the compartment. Variation of peak temperature in the compartment and its location with fire size for steel and concrete beams is shown in Fig. 9. The location of peak temperature x^* is represented as the ratio of the distance along the fire path from the origin of the fire to the total length of the fire path as in Eq. (20).

$$x^* = x/L \tag{20}$$

The highest peak temperature differences along the fire path are found for fire sizes larger than 10%. Fig. 8 shows that for smaller fire sizes, temperature variations across the length are minimal, except for the compartment ends where fire growth and extinction are assumed to occur. The reasons for low variability in peak temperatures along the compartment for small fires are slow fire spread rate and resultant long pre-heating periods. The exposure to high gas temperatures for small fires is long enough for steel to reach similar high peak temperatures everywhere. On the other hand, in the case of larger fires (>10%) fire spread rate is much faster. Therefore, structural elements close to fire origin experience pre-heating only for a very short duration. This duration is not long enough for structural elements to heat up to peak temperatures as at the far end. Thus, variation of peak steel temperatures along the compartment is in the range of 60–170 °C.

It can be seen from both Figs. 8 and 9 that for all fire sizes the peak steel and concrete temperatures occur at the locations further than $x^* = 0.6$ L from the fire origin. For very small fire sizes (<2%) a sudden increase of distance from fire origin with fire size can be seen. As identified previously, for such small fires the peak temperatures vary little. This can be seen from the 5 °C variation from the peak temperature shaded region. Thus, high variation in location of peak temperatures can be neglected.

For larger fires with increasing fire sizes the distance of location of peak temperatures from the fire origin in both steel and concrete members is decreasing up to fire sizes of 25–33%. It represents the location slightly further than where the fire size starts to decrease. The reason for that is that members up to that location are exposed to the same far-field temperatures for increasing durations. However, as the fire

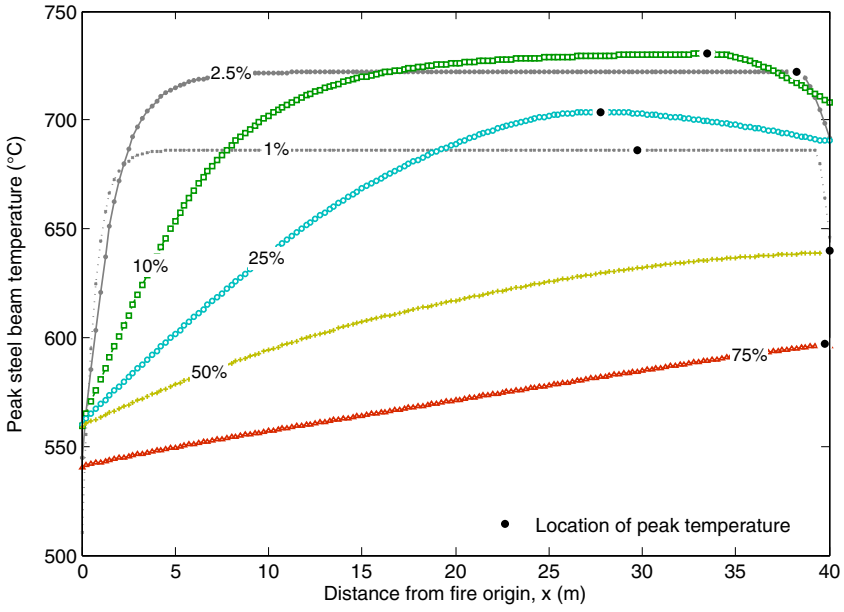

Fig. 8. Peak 60 min protected steel beam temperatures along the fire path for different fire sizes. Highlighted points on the curves indicate the location of the peak temp.

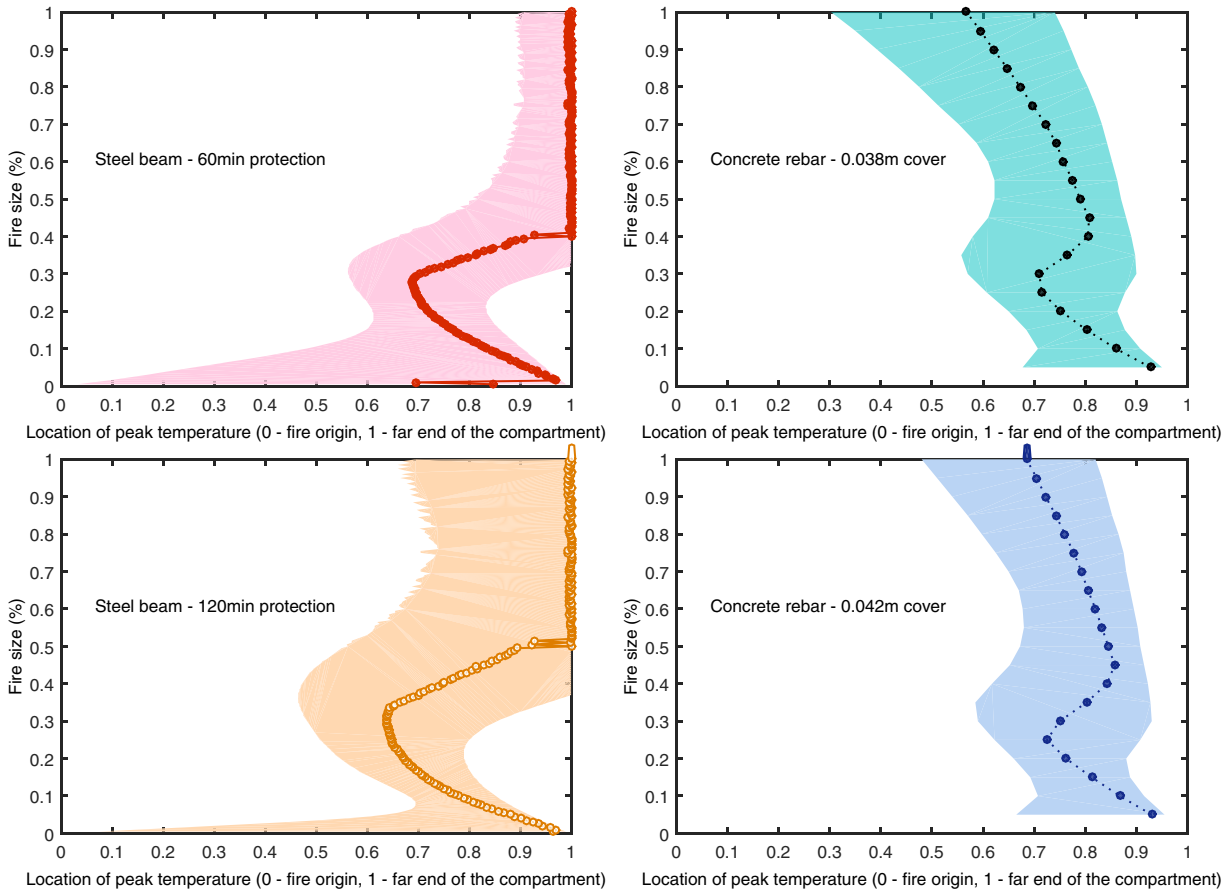

Fig. 9. The peak steel and concrete rebar temp. And their location in the compartment from the fire origin (a ratio to the full fire length) for various fire sizes; Shaded region displays locations of max temp. within 5 °C difference from the peak temp.

starts to decay the members at the far end of the compartment are exposed to peak near-field temperatures for shorter durations as well as lower far-field temperatures during cooling. Thus, the resulting temperatures are lower at the end and peak temperature occurs at the location close to where fire decay begins.

On the other hand, fires larger than approximately 25% are large enough to produce high smoke temperatures above the temperatures of the beams. Thus, the temperatures at the far end of the compartment keep on significantly increasing even during the decay phase. In addition to that, steel temperatures for larger fires are lower than for smaller fire sizes due to faster fire spread rates (see Fig. 8) and are exposed to shorter cooling durations. Therefore, as seen in Figs. 8 and 9, the distance from the fire origin of the peak temperature starts to increase for large fire sizes. Though, for concrete rebar the location of the peak temperature in the compartment for fires larger than 40% of floor area decreases.

It can be concluded that the location of the peak temperature in the compartment is a function of both the fire size (i.e. heat release rate and resulting smoke temperatures) and spread rate (i.e. time, for which structural members are exposed to pre-heating). For fire sizes smaller than 25% the effects of fire spread rate are more dominant while for larger fires the size of the fire becomes more dominant.

Fig. 10 shows variation of the location of the peak temperature in the compartment for different heat release rates. For both steel and concrete rebar the higher the heat release rate or the thickness of fire protection (see Fig. 9) the closer the location to the fire origin. The thicker the fire protection, the slower the response to the changes in gas temperatures. Other parameters such as length of the fire compartment, fuel load density and flapping angle were varied as well. However, no influences on the location of peak temperature from the fire origin have been observed as these parameters varied.

5. Conclusions

Current design codes invoke gas time–temperature curves which are based on small enclosure fires. Uniform temperature distributions in the compartments are proposed while in real buildings, fires have been observed to travel. The World Trade Centre Tower fires in 2001 have highlighted the need of a more realistic design tools to represent fires in large compartments. Travelling Fires Methodology has been developed to account for the travelling nature of fires. In this study the TFM

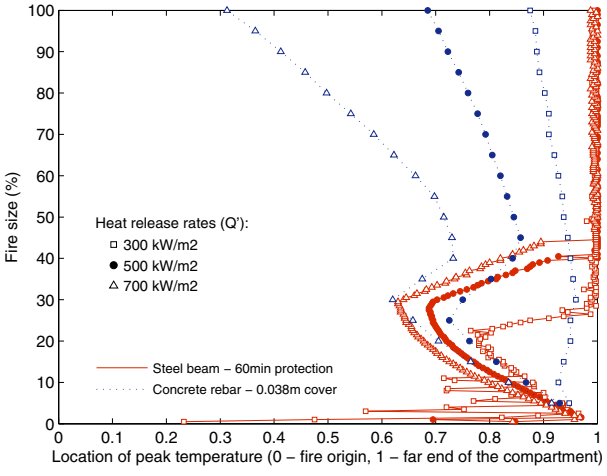

Fig. 10. Variation of location of peak steel and concrete rebar temperatures in the compartment for heat release rates per unit area $Q^{*'}$ of 300 kW/m^2, 500 kW/m^2 and 700 kW/m^2.

has been refined based on better fire model and used to analyse thermal gradients in a simple structure.

The introduced limitation on the range of possible fire sizes reduces the computational time required by eliminating unrealistic fire coverage areas based on fire spread rates observed in experiments and real fires. Analytical correlation presented for generation of gas time–temperature curves is independent of grid size and can be easily calculated with any mathematical tool. Also, introduction of flapping term leads to reduced near-field temperatures for smaller fire sizes which cover a range between 800 and 1200 °C observed in real building fires. The occurrence of peak member temperatures for fire sizes in the range of 5 to 20% diminishes with increasing flapping angle.

Finally, the location of the peak temperature in the compartment is found to occur at the end of the fire path (i.e. >0.6 L).It is dominated by fire spread rate for small fire sizes up to 30% although it depends on the thickness of fire protection and heat release rate. Total heat release rate becomes more dominant for large fires.

The proposed changes represent a crude fire model which can be used flexibly and updated as the new data becomes available. More experimental evidence in large compartments is necessary for further development and improvements.

Acknowledgements

The research has been funded by the Engineering and Physical Sciences Research Council (EPSRC, UK) with grant number EP/K502856/1, Ove Arup and Partners Limited (UK), Centre d'Études et de Recherches de l'Industrie du Béton (CERIB, France) and Educational & Scientific Foundation of the Society of Fire Protection Engineers (SFPE, USA). The authors appreciate the valuable technical discussions held with Mohammad Heidari and Panos Kotsovinos. Data supporting this publication can be obtained from http://dx.doi.org/10.5281/zenodo.18873 under a Creative Commons Attribution license.

Appendix A. Flapping angle

Quintiere et al. [39] carried out experiments to study the effects of openings in the room on fire plume entrainment. One of the measurements taken was flame angle. It can be seen from their results that the measured angle was not constant but rather was fluctuating with time. For all experiments, variation of flame angle was between ±4° and ±15° with an average value of ±6.5° independent of fire size. For this study an effort was made to measure the angles (i.e. the length over which the flame fluctuates in relation to fuel base) from the published photographs of oscillating flame plumes in various experiments [38,44–47]. The maximum angle amplitude was in a range of [±3 to ±15]° (see Table A1). In most of these experiments the maximum effort was taken to avoid any disturbances. The measured average angles were also plotted against the dimensionless heat release rate, which is shown in Fig. A.1. However, no significant dependency between the two was observed. It can be seen that the measured angle only minimally increases with higher heat release rates. Thus, for the updated version of TFM the flapping angle of ±6.5° was chosen based on results from Quintiere et al. [39] experiments. It also falls within the range of other measured values.

Table A1
Flapping angles based on data published in literature.

Ref.	Year	Angle (°)	$-\Delta\theta_{,max}$ (°)	$+\Delta\theta_{,max}$ (°)	*Fr*	$Q^{\bullet}$ (kW)	*D* (m)		Q^{*}	Fuel
[39]	1981	6.5	2.5	8.5	–	62.9	0.3	○	1.16	Methane
		5.6	1.6	4.4	–	158	0.3	○	2.91	Methane
[44]	2011	7.6	1.1	2.2	0.695	–	1.32	○	162.5	Propane
		6.7	1	1.1	0.742	–	1.32	○	167.9	Propane
[47]	2012	4.7	3.7	2.3	–	–	0.30	□	–	n-Heptane
[38]	1984	2.3	0.3	0.7	0.000117	28	0.25	○	0.81	Methane
		5.7	1.7	1.3	8.66E−05	54	0.34	□	0.74	Methane
[45]	1979	4.3	3.3	4.7	–	33	0.34	□	0.45	Methane
[46]	1993	3.4	2.4	4.6	–	60	0.3	○	1.11	Propane
		5.8	0.8	1.2	–	3	0.3	○	0.06	Propane

Fr — Froude number; *D* — fire source diameter; Q^{*} — dimensionless heat release rate.

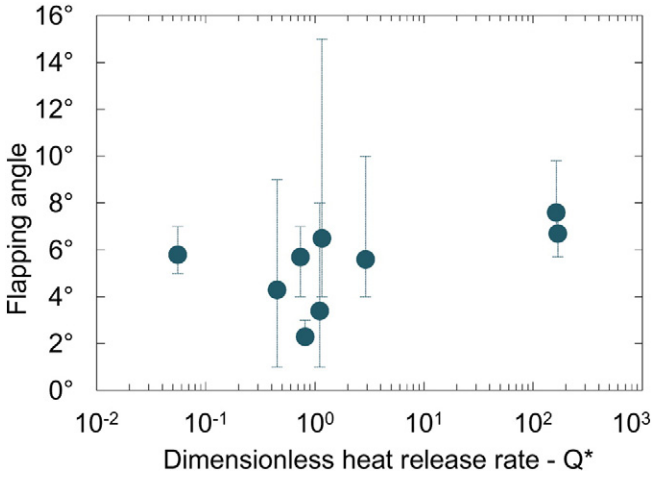

Fig. A.1. Relationship of flapping angle measures based on the data published in the literature with dimensionless heat release rate.

Appendix B. Calculation of reduced near-field temperature

Reduced near-field temperature due to flapping is calculated by taking an average gas temperature over the flapping length as shown in Fig. B.1. The far-field temperature function is integrated from the near-field edge to the flapping length edge, near-field temperatures over fire length are added, and an average reduced near-field temperature is calculated, see Eq. (21).

$$T_f = (A_{ff} + 1200L_f)/f \tag{21}$$

where T_f is the reduced near-field temperature (°C) and A_{ff} is a sum of far-field temperatures in the region of flapping length. The latter is calculated by integrating Alpert's correlation [28] from the end of the flapping length ($r_2 = f/2$) to the end of the fire length ($r_1 = L_f/2$). The far-field limits r_1 and r_2 are represented in Fig. B.1.

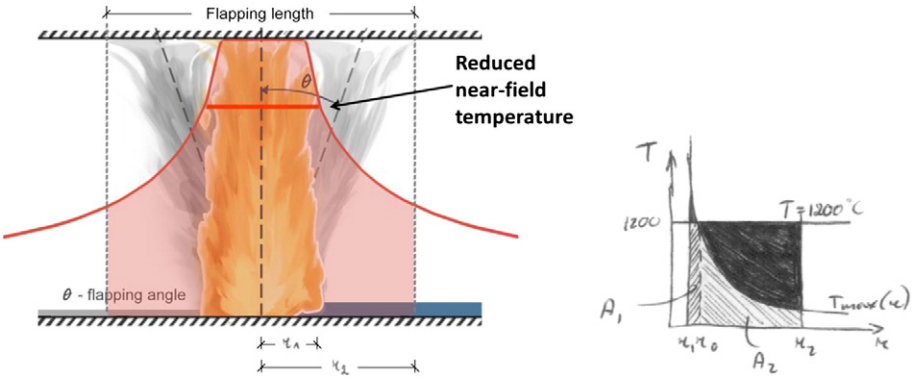

Fig. B.1. Region over which gas temperatures are averaged to find a reduced near-field temperature (left); and limits of integration for calculating the average of far-field temperatures over the flapping length (right).

Using Alpert's correlation function [28] the near-field temperatures over a certain distance might be higher than a set maximum near-field temperature of 1200 °C. These higher temperatures in TFM are reduced to maximum near-field temperature. This introduces another variable r_0, which is required for integration of far-field temperature function and does not allow far-field temperatures to be higher than a near-field temperature. r_0 is the crossing point between gas temperatures obtained using Alpert's correlation function [28] and near-field temperature of 1200 °C.

$$T_{nf} = T_\infty + 5.38\frac{(Q^{\bullet}/r_0)^{2/3}}{H} \tag{22}$$

$$r_0 = \left(\frac{5.38}{H(T_{nf} - T_\infty)}\right)^{3/2} \tag{23}$$

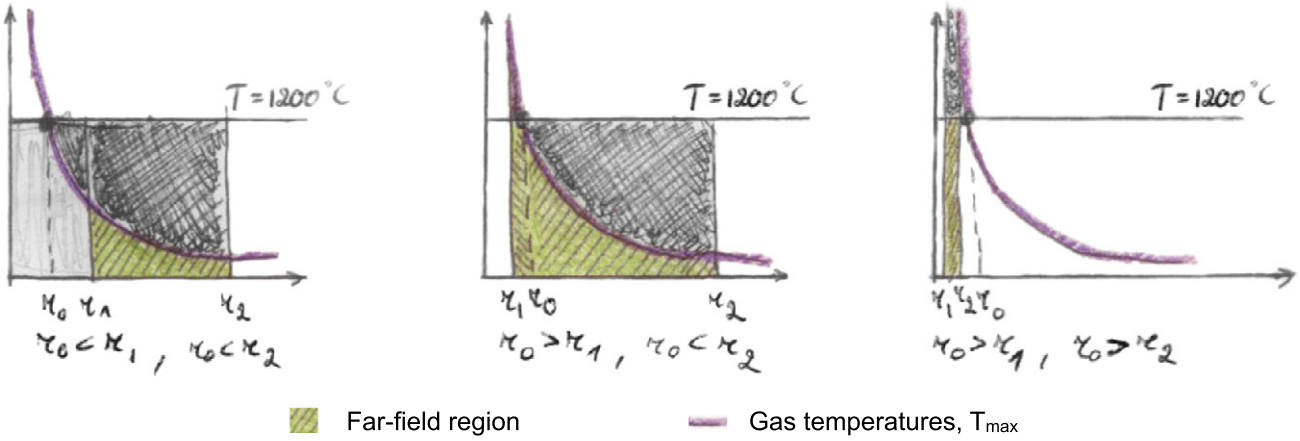

Fig. B.2. The three possible different scenarios for the location of r_0 in relation to the location of the near-field edge r_1, and the location of the flapping length edge r_2.

There are three possible crossing point r_0 locations in relation to near-field edge r_1 and flapping length edge r_2. They are shown in Fig. B.2. Thus, the sum of far-field temperatures over the flapping length can be calculated as follows:

$$A_{ff} = 2(A_1 + A_2) \tag{24}$$

$$A_1 = T_{nf} \cdot r_{x1} \tag{25}$$

$$A_2 = \int_{r_{x2}}^{r_2} T_{max}(r)dr = \int_{r_{x2}}^{r_2}\left(T_\infty + 5.38\left(\frac{Q^{\bullet}/r)^{2/3}}{H}\right)dr = T_\infty(r_2 - r_{x2}) + \frac{16.14Q^{\bullet 2/3}}{H}\left({r_2}^{1/3} - {r_{x2}}^{1/3}\right) \quad (26)$$

$$r_{x1} = \max[0, r_0 - L_f/2] \quad (27)$$

$$r_{x2} = \max[L_f/2, r_0] \quad (28)$$

where A_1 is the sum of temperatures, when those in the far-field calculated using Alpert's equation [28] are above the near-field temperature and the length over which this occurs is defined by r_{x1}. A_2 is the sum of temperatures, when those in the far-field calculated using Alpert's equation [28] are below the near-field temperature. This is done by integrating over the limits of flapping length edge r_2 and r_{x2}. r_{x2} defines the lower limit based on where the crossing point r_0 is located (see Fig. B.2). Therefore, combining the Eqs. (21)–(26) the reduced near-field temperature due to flapping can be calculated as in Eq. (29).

$$T_f = T_\infty + \frac{T_{nf}(2r_{x1} + L_f) - 2T_\infty \cdot r_{x2}}{f} + \frac{32.28Q^{\bullet 2/3}}{H \cdot f}\left({r_2}^{1/3} - {r_{x2}}^{1/3}\right) \quad (29)$$

Appendix C. Supplementary data

Supplementary data to this article can be found online at http://dx.doi.org/10.1016/j.istruc.2015.06.001.

References

[1] Hall JR, (NFPA). Burns, toxic gases, and other fire-like hazards in non-fire situations; 2004.
[2] Butry DT, Chapman RE, Huang AL, Thomas DS. A life-cycle cost comparison of exit stairs and occupant evacuation elevators in tall buildings. Fire Technol 2012;48:155–72. http://dx.doi.org/10.1007/s10694-010-0203-8.
[3] Buchanan AH, 2001 'Structural design for fire safety', John Wiley & Sons, Ltd.
[4] Flint G, Lamont S, Lane B, Sarrazin H, Lim L, Rini D, et al. Recent lessons learned in structural fire engineering for composite steel structures. Fire Technol 2013;49:767–92. http://dx.doi.org/10.1007/s10694-012-0291-8.
[5] Kirby BR, 1998 'The behaviour of a multi-storey steel framed building subjected to fire attack experimental data', British Steel PLC, Rotherham
[6] Newman GM, Robinson JT, and Bailey CG, 2006 'Fire safe design: a new approach to multi-storey steel-framed buildings', (second edition) The Steel Construction Institute, Ascot
[7] Stern-Gottfried J, Rein G. Travelling fires for structural design—part I: literature review. Fire Safety J 2012;54:74–85. http://dx.doi.org/10.1016/j.firesaf.2012.06.003.
[8] Stern-Gottfried J, Rein G. Travelling fires for structural design—part II: design methodology. Fire Safety J 2012;54:96–112. http://dx.doi.org/10.1016/j.firesaf.2012.06.011.
[9] Franssen J-M. Improvement of the parametric fire of Eurocode 1 based on experimental test results. Fire Safety Sci 2000;6:927–38. http://dx.doi.org/10.3801/IAFSS.FSS.6-927.
[10] McAllister TP, Gross JL, Sadek F, Kirkpatrick S, MacNeill RA, Zarghamee M, et al. Structural response of World Trade Center buildings 1, 2 and 7 to impact and fire damage. Fire Technol 2013;49:709–39. http://dx.doi.org/10.1007/s10694-012-0289-2.
[11] Gann RG, Hamins A, McGrattan K, Nelson HE, Ohlemiller TJ, Prasad KR, et al. Reconstruction of the fires and thermal environment in World Trade Center buildings 1, 2, and 7. Fire Technol 2013;49:679–707. http://dx.doi.org/10.1007/s10694-012-0288-3.
[12] Post NM. 9/11 blazes debunk code assumptions about fire behavior in open-plan offices' Engineering News Record; 2013.
[13] Clifton CG. Fire models for large firecells. HERA Report R4-83; 1996.
[14] Law A, Stern-Gottfried J, Gillie M, Rein G. The influence of travelling fires on a concrete frame. Eng Struct 2011;33:1635–42. http://dx.doi.org/10.1016/j.engstruct.2011.01.034.
[15] Rein G, Zhang X, Williams P, Hume B, Heise A, Jowsey A, et al. Multi-storey fire analysis for high-rise buildings. 11th International Interflam Conference; 2007 http://hdl.handle.net/1842/1980.
[16] Law A, Butterworth NA, Stern-gottfried J, Wong Y. Structural fire design: many components, one approach. 1st International Conference on Performance Based Life Cycle Structural Engineering; 2012.
[17] Law A, Stern-Gottfried J, Butterworth N. A risk based framework for time equivalence and fire resistance. Fire Technol 2015;51(4):771–84. http://dx.doi.org/10.1007/s10694-014-0410-9.
[18] Kirby BR, Newman GM, Butterworth N, Pagan J, and English C, 2004 'A new approach to specifying fire resistance periods', Struct Eng, pp 34–37.
[19] Gales J. Travelling fires and the St. Lawrence Burns project. Fire Technol 2014;50(6):1535–43. http://dx.doi.org/10.1007/s10694-013-0372-3.
[20] Williams-Leir G. St. Lawrence Burns Temperature Measurements. National Research Council Canada: Research Report; 1959. http://dx.doi.org/10.4224/203866508. DBR-IR-152.
[21] Eurocode 1: actions on structures — part 1-2: general actions — actions on structures exposed to fire. Brussels: CEN: European Standard EN 1991-1-2; 2002.
[22] Nelson HE. An engineering view of the fire of May 4, 1988 in the First Interstate Bank building Los angeles, California; 1989.
[23] Thomas PH. Some aspects of the growth and spread of fire in the open. Forestry 1967;40:139–64. http://dx.doi.org/10.1093/forestry/40.2.139.
[24] Quintiere JG, 1998 'Principles of fire behaviour', Cengage learning
[25] Kirby BR, Wainman DE, Tomlinson LN, Kay TR, Peackok BN. Natural fires in large scale compartments — a British steel technical. Fire Research Station collaborative project; 1994.
[26] Routley JG. Interstate bank building fire'Los Angeles; 1988.
[27] Passive systems and building fire safety design — Task group six report; Fire Safety and Engineering. Technical Papers, Book Two Sydney, Australia; 1989.
[28] Alpert RL. Calculation of response time of ceiling-mounted fire detectors. Fire Technol 1972;8:181–95. http://dx.doi.org/10.1007/BF02590543.
[29] Suzuki K. Unsteady ceiling jet model for large building spaces. Fire Safety J 2013;61:83–91. http://dx.doi.org/10.1016/j.firesaf.2013.08.007.
[30] Johansson N, Wahlqvist J, and van Hees P, 2014 'Numerical experiments in fire science: a study of ceiling jets', Fire Mater. doi: http://dx.doi.org/10.1002/fam.2253
[31] Alpert RL. Turbulent ceiling-jet induced by large-scale fires. Combust Sci Technol 1975;11:197–213. http://dx.doi.org/10.1080/00102207508946699.
[32] Heskestad G. Physical modeling of fire. J Fire Flammability 1975;6:253–73.
[33] Thomas PH. Fires in enclosures. In: Blackshear PL, editor. Heat Transf. Fires Thermophys. Soc. Asp. Econ. Impact. Washington: Building Research Establishment; 1974. p. 13.
[34] Drysdale D. An introduction to fire dynamics3rd ed. ; 2011. http://dx.doi.org/10.1002/9781119975465.
[35] Kirby BR, Wainman DE, Tomlinson LN, Kay TR, Peacock BN. Natural fires in large scale compartments. Int. J. Eng. Performance Based Fire Codes, 1; 1999. p. 43–58.
[36] Lennon T, Moore D. The natural fire safety concept—full-scale tests at Cardington. Fire Safety J 2003;38:623–43. http://dx.doi.org/10.1016/S0379-7112(03)00028–6.
[37] Santoni P-A, Marcelli T, Leoni E. measurement of fluctuating temperatures in a continuous flame spreading across a fuel bed using a double thermocouple probe. Combust Flame 2002;131:47–58. http://dx.doi.org/10.1016/S0010-2180(02)00391–7.
[38] Crauford NL. The structure of an unconfined buoyant turbulent diffusion flame. University of Southampton; 1984.
[39] Quintiere JG, Rinkinen WJ, Jones WW. The effect of room openings on fire plume entrainment. Combust Sci Technol 1981;26:193–201. http://dx.doi.org/10.1080/00102208108946960.
[40] Eurocode 3: design of steel structures — part 1-1: general rules and rules for buildings. European Standard EN 1993-1-1. Brussels: CEN; 2005.
[41] Eurocode 2: design of concrete structures — part 1-1: general rules and rules for buildings. European Standard EN 1992-1-1. Brussels: CEN; 2004.
[42] Incropera F, DeWitt D, Bergman T, and Lavine A, 2007 'Fundamentals of heat and mass transfer', John Wiley & Sons, Ltd.
[43] Forrest JCM. The whole structure. In: Anchor RD, Malhotra HL, Purkiss JA, editors. Int. Conf. Des. Struct. Against Fire. Birmingham: Elsevier Applied Science Ltd.; 1986. p. 111–25.
[44] Langman AS, Nathan GJ. Influence of a combustion-driven oscillation on global mixing in the flame from a refinery flare. Exp Thermal Fluid Sci 2011;35:199–210. http://dx.doi.org/10.1016/j.expthermflusci.2010.09.002.
[45] McCaffrey BJ. Purely buoyant diffusion flames: some experimental results. National Bureau of Standards Report NBSIR 79-1910; 1979 Washington.
[46] Cetegen BM, Ahmed TA. Experiments on the periodic instability of buoyant plumes and pool fires. Combust Flame 1993;93:157–84. http://dx.doi.org/10.1016/0010-2180(93)90090-P.
[47] Chen J, Bao Q. Digital image processing based fire flame color and oscillation frequency analysis. Protein Eng 2012;45:595–601. http://dx.doi.org/10.1016/j.proeng.2012.08.209.